2018•2019

Faculteit Industriële ingenieurswetenschappen

master in de industriële wetenschappen: chemie

Masterthesis

Improvement of an aerosol photoreactor operation

PROMOTOR :

De heer Mumin Enis LEBLEBICI

PROMOTOR :

Prof. dr. ir. Leen BRAEKEN

BEGELEIDER :

ir. Emine KAYAHAN

Jarred Aussems

Scriptie ingediend tot het behalen van de graad van master in de industriële wetenschappen: chemie

Gezamenlijke opleiding UHasselt en KU Leuven

2018 • 2019

Faculteit Industriële ingenieurswetenschappen

master in de industriële wetenschappen: chemie

Masterthesis

Improvement of an aerosol photoreactor operation

PROMOTOR :

De heer Mumin Enis LEBLEBICI

PROMOTOR :

Prof. dr. ir. Leen BRAEKEN

BEGELEIDER :

ir. Emine KAYAHAN

Jarred Aussems

Scriptie ingediend tot het behalen van de graad van master in de industriële wetenschappen: chemie

UHASSELT KU LEUVEN

Preface

This thesis is the final test in my education to achieve my Master of Chemical Engineering Technology. In this thesis, I will discuss the improvement of a new photoreactor operation: an aerosol photoreactor. The reason why I choose this subject was to test myself and help developing something new. Due to the small amount of literature and information on the subject, it was challenging for me with many ups and downs. Although I will miss studying, I am looking forward to exploring the chemical industry.

First of all, I want to thank my promotor Prof. Dr. Ir. Mumin Enis Leblebici. Because of his knowledge about aerosol photoreactors, I learned many things about this subject and could always ask him for advice. I also want to thank my mentor Ir. Emine Kayahan who was, in addition to her role of mentor, a promotor for me. She taught me how to operate the reactor and always helped me during the countless setbacks I had during my internship. She also taught me how to write a concise and scientific thesis.
I wish Emine the best of luck with the progress and completion of her PhD. In addition, I would like to thank Ing. Mathias Jacobs and all the employees of lab4U because I could always count on them. I would like to thank my fellow master's students for the many conversations during the breaks.

I also want to thank my friends and family for their trust and support. Lastly, I want to thank my girlfriend. I could always count on her both during my studies and my master's thesis.

Jarred Aussems

Diepenbeek, June 10th, 2019

Table of contents

List of tables

List of figures

Abstract

Aerosol photoreactors present themselves as promising candidates for industrial applications to solve the problem of current photo microreactors not being able to simultaneously have a high reaction rate and high throughput. Although promising, such reactors need characterization and optimization. The aim of this thesis was to optimize the reactor operation: the transformation from batch to a continuous reactor, integration of a humidity sensor, improvements in aerosol separation and tests on the lamp reliability.

The reactor using a continuous nebulizer was operated to generate a continuous aerosol flow. A pump, a flow sensor and a control unit were implemented to control the flow. A humidity sensor and an Arduino were utilized to measure humidity. The residence time distribution (RTD) was characterized for different gas and liquid flow rates. Hydrophobic (polyethylene) and hydrophilic (glass) filters were compared for aerosol separation. The fluctuation of a gas-discharge tube and LED strips was determined in length and in time.

Polyethylene and glass filters give similar results. Glass is chosen due to its chemical inertness. The gas-discharge tube and the LEDs have a maximum fluctuation of respectively 21 $\mu W/(cm^2.nm)$ and 0.57 $\mu W/(cm^2.nm)$ in length. In time, the fluctuation for both lamps is negligible. Average residence times of a few seconds are achieved for different parameters.

Abstract in het Nederlands

Aerosol-fotoreactoren presenteren zich in de industrie als veelbelovende kandidaten om de problemen van huidige foto-microreactoren, die een hoge reactiesnelheid en een hoge productie niet gelijktijdig kunnen verwezenlijken, op te lossen. Hoewel ze veelbelovend zijn, moeten dergelijke reactoren verder gekarakteriseerd en geoptimaliseerd worden. Het doel van deze masterproef was dan ook de optimalisatie van deze reactor: de overgang van batch naar een continue reactor, integratie van een vochtigheidssensor, verbetering van aerosolscheiding en het testen van de betrouwbaarheid van de lamp.

De reactor, gebruik makende van een continue vernevelaar, werd gebruikt om continu aerosol te genereren. Een pomp en een debietsensor met regeleenheid werden geïmplementeerd om het debiet te regelen. Een vochtigheidssensor en een Arduino werden gebruikt om de vochtigheid te meten. De verblijftijdspreiding werd gekarakteriseerd voor verschillende gas- en vloeistofdebieten. Hydrofobe (polyethyleen) en hydrofiele (glas) filters werden vergeleken in de aerosolscheiding. De fluctuatie van een gasontladingslamp en led-strips werd bepaald in de lengte van de lamp en in de tijd.

Beide filters geven vergelijkbare resultaten. Glas filters zijn gekozen omdat ze chemisch inert zijn. De gasontladingslamp en leds hebben een maximale fluctuatie van respectievelijk 21 µW/(cm².nm) en 0.57 µW(cm².nm) in de lengte. De fluctuatie in tijd is verwaarloosbaar. Gemiddelde verblijftijden van enkele seconden zijn behaald voor verschillende parameters.

1. Introduction

1.1. Background

Photochemical reactions are chemical reactions that are initiated by the absorption of energy in the form of UV-light, visible light or infrared radiation. Photochemical transformations of molecules provide access to reaction pathways that are impossible to reach with classical thermochemical activation. In addition, photochemical reactions are performed at mild temperatures. In spite of these advantages, photochemistry is not often used in industry due to sub-optimal reactor designs.

In an ideal photoreactor, light utilization is maximized. There are no dark regions inside the reactor and no light is wasted. The ideal photoreactor design must overcome the mass transfer and photon transfer limitations. The performance and efficiency of different photoreactors can be compared with a benchmark: photocatalytic space time yield (PSTY). PSTY gives information on the volume or mass of product per time per reactor volume and per energy input ($m^3/(day.m^3.kW)$ or $kg/(day.m^3.kW)$). An optimum reactor operation should result in a high PSTY [1].

Among the photo microreactors, a novel micro structured reactor – the aerosol photoreactor – is a quite promising candidate. An aerosol photoreactor uses a nebulizer to nebulize the reaction medium with an inert or reacting gas as droplets of µm scale. Each droplet functions as a microreactor. In literature, there is little information about this reactor and it is only operated twice.

In this thesis, the operation of an aerosol photoreactor was improved.

1.2. Problem description

An aerosol photoreactor is a quite promising candidate among the photo microreactors due to the possibility of this technology to boost the reaction rates. However, operational parameters such as air pressure and liquid flow rate affect the reactor performance. In addition, the nebulizer type affects the reactor performance. In order to get information on the mixing and the reactor performance, it is important to characterize the residence time distribution of various aerosol photoreactors.

Two reactors were studied with similar designs but different nebulizers: a medical nebulizer and a continuous nebulizer. A medical nebulizer can be filled with a maximum of 10 ml. The reactor can be run for 10 ml of liquid each operation and is therefore a batch set-up. A continuous nebulizer, on the other hand, can be operated continuously. Therefore, in this work, the existing reactor using a medical nebulizer was replaced with a new reactor using a continuous nebulizer to transform the process from batch to continuous. Improvement of this reactor set-up was necessary in order to improve the reactor operation. A continuous separation unit operation, which is the separation of the liquid and the gas phase of the aerosol, was one of the main problems of the set-up. The humidity inside the reactor was also a problem. The size of aerosol droplets is micro-scale, they evaporate easily if the reactor is not saturated. This will result in a lower and inconsistent throughput. Therefore, the humidity inside the reactor needed to be measured. Lamp reliability is also an important part in the operation of an aerosol photoreactor. Fluctuations in the length of the lamp and in time can cause inefficient operation.

1.3. Objectives

The main objective of this thesis was to improve the aerosol photoreactor operation:

- transformation of the aerosol photoreactor operation from batch to continuous;
- implementation of a humidity sensor to measure the humidity inside the reactor;
- determination of a suitable continuous phase separation operation;
- measurement of the lamp reliability;
- measurement of the residence time distribution.

1.4. Materials and methods

Two different reactors were studied. The first reactor used a medical nebulizer that can be purchased in an apothecary. Only the air flow rate could be controlled with this nebulizer. The nebulizer was filled with maximum 10ml liquid sample where air was passed through to nebulize the liquid. The second reactor had the same dimensions but utilized a different nebulizer: a Burgener Teflon mira mist nebulizer. Both the liquid and air flow could be controlled with this nebulizer. The latter one was more practical to use in continuous operations.

The existing set-up using the medical nebulizer was improved and the new set-up using the continuous nebulizer was assembled afresh after gathering the required components. Both set-ups were improved with a humidity sensor and a pressure safety valve. A peristaltic pump, a flow sensor and a PID-controller were implemented to the system using the continuous nebulizer to provide liquid to the nebulizer. To determine a proper separation unit at the end of the reactor, hydrophobic (glass) and hydrophilic (polyethylene) filters with different pore sizes were studied. A humidity sensor was installed in the reactor and connected to an Arduino to measure the humidity when only air was flowing in the reactor and when aerosol was flowing in the reactor.

To measure the lamp reliability and to maximize the light utilization, the radiant flux received by a surface per unit area, also called the absolute spectral irradiance, was measured for two lamps: a gas-discharge tube and LED strips. The irradiance was measured in six points distributed over the length of the lamps and in one point during one hour.

The residence time distribution was characterized for various operational parameters. The performance of an aerosol photoreactor depends on the aerosol concentration and the droplet size. The droplet size could be controlled by changing the air pressure: the greater the air pressure, the smaller the droplet size. Larger droplets were expected to go out of the reactor more quickly since they were heavier. The residence time distribution was determined by measuring the transmission at the reactor outlet. A Maya 2000pro spectrometer was connected to a flow cell at the end of the reactor to measure the transmission. The transmission dropped as more aerosol droplets flow out of the reactor until a steady-state was formed in the reactor.

2. Literature study

2.1. Light

Visible light is part of the electromagnetic radiation (Fig. 1). Light has a wave-particle duality. In other words, it can behave as both a particle and a wave. As a particle, light can be observed as packages of energy moving at the speed of light. Each package is called a photon. Light also has the properties of a wave: a frequency and a wavelength. As shown in Fig. 1, light has a broad range of wavelengths which can be represented in an electromagnetic spectrum [2].

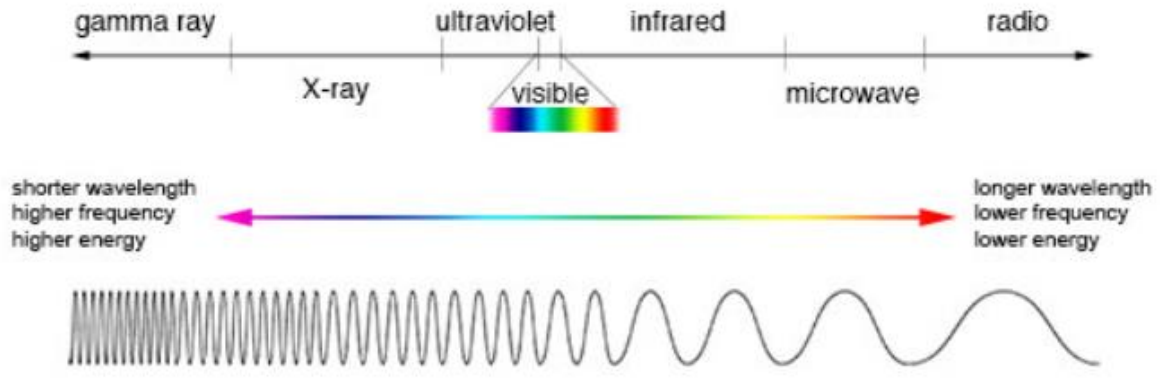

Fig. 1. Electromagnetic spectrum [3]

The wavelength and frequency are related to each other:

$$v = f\lambda \tag{1}$$

where v is the velocity at which the wave is travelling through the matter ($m.s^{-1}$), f is the frequency (Hz) and λ is the wavelength (m). The velocity of light is dependent on the medium in which the light is travelling. In vacuum, the velocity of light is 3.00×10^8 m/s.

As shown in Fig. 1 and according to equation 1, as the wavelength of light is smaller and the frequency is higher, the energy of the photons is higher.

The radiative energy in the form of UV-light, visible light and infrared radiation can be absorbed by reagents and initiate a photochemical reaction. The reagents will create an excited state in which the molecules can react and form the desired end product.

2.2. Photochemistry & flow chemistry

The Beer-Lambert-Bouguer law is an important law in photochemistry:

$$I = I_0 e^{-c\varepsilon b} \tag{2}$$

Where I is the spectral irradiance ($W.m^{-2}.nm^{-1}$) at light-path thickness b (m), I_0 is the spectral irradiance before the absorption ($W.m^{-2}.nm^{-1}$), c is the concentration of the absorbing specie ($mol.l^{-1}$) and ε is the molar absorptivity ($l.mol^{-1}.m^{-1}$) [4].

According to equation 2, spectral irradiance decreases exponentially. A photoreactor with a large light-path thickness results in a lower chemical conversion since the penetration of the light into the photoreactor is not deep enough. In conclusion, the productivity of a photoreactor decreases exponentially with decreasing rate of absorbed radiative energy.

2.2.1. Comparison of the photoreactor performance: Space time yield, quantum efficiency and photochemical space time yield

In literature, several photoreactors are being used and compared. Several benchmarks are used to compare the reactor performance: Space time yield, quantum efficiency and the photochemical space time yield.

Space time yield (STY) is the measure of productivity in a photoreactor design and can be given as;

$$STY = \frac{m_p}{V_r \times t} \tag{3}$$

where m_p is the mass of formed product (g), V_r is the reactor volume (l) and t is the time (day). STY only gives a measure of productivity. If the energy of the lamp is included in this definition, the photocatalytic space-time yield (PSTY) can be defined. The energy of the lamp, the lamp power, can be calculated using the following relation;

$$LP = P \times \frac{1l}{V_r} \tag{4}$$

where LP is the standardized lamp power (W or kW), P is the lamp power of the setup (W or kW). The PSTY is defined as;

$$PSTY = \frac{STY}{LP} \tag{5}$$

The STY represents the productivity of a photoreactor (mass or volume of product per time per reactor volume) and PSTY represents the efficiency of a photoreactor (mass or volume of product per time per reactor volume per unit energy input). The changes in the efficiency, product throughput and productivity with respect to the light path are shown in Fig. 2.

Fig. 2a shows that a longer light path through the reaction medium results in a decrease of the productivity of the photoreactor. The efficiency however increases until the path length is 25 mm before it decreases like the productivity. The product throughput (Fig. 2d), which is calculated by multiplying STY by the volume of the reaction mixture, increases until a certain path length. The maximum PSTY coincides with the maximum throughput. This proves that the PSTY is a good benchmark when trying to achieve an optimum reactor operation [1].

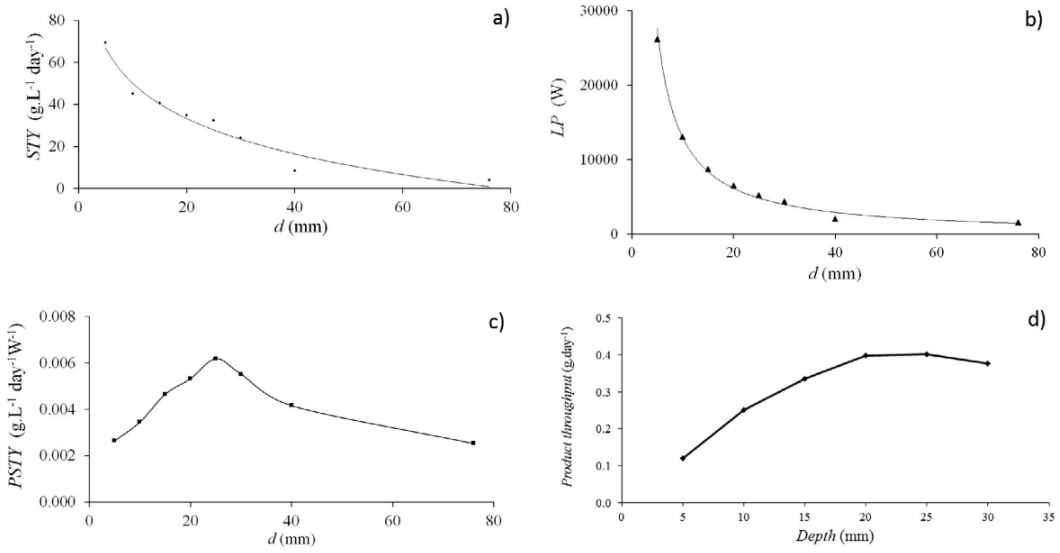

Fig. 2. STY (a), LP (b), PSTY (c) and product throughput (d) with respect to light-path length [1]

2.2.2. Photo microreactors

Fourteen different photoreactors with 12 different designs for wastewater treatment were compared using PSTY in a previous study [5]. A schematic view of 10 designs are given in Fig. 3. The 2 missing designs are a continuous stirred tank reactor and a slurry version of the foam reactor. Hybrids which combine different designs were also used in this article. These reactors had been proposed to overcome the limitations of the suboptimal design of a photoreactor: mass transfer limitation and photon transfer limitation. The different reactor designs were divided in two groups: the slurry photoreactors and the photoreactors using an immobilized catalyst. A slurry photoreactor can be used to react solids, liquids and gases simultaneously. Usually it consists of solids suspended in a liquid, through which a gas is bubbled. The photocatalyst is added to the slurry and is eventually separated from the slurry at the end of the reactor. In a photoreactor using an immobilized catalyst, the catalyst is not added to the slurry but is immobilized inside the reactor by coating it on the reactor wall for example [6].

When looking at Table 1, the author concluded that the highest PSTY (0.72) was achieved using a hybrid of two slurry reactors: a photocatalytic membrane reactor and a multi-lamp reactor. Both reactors are continuous. In a photocatalytic membrane reactor, a membrane is used to separate the catalyst from the slurry. The catalyst is then recycled in the reactor [7]. A multi-lamp reactor is a tubular reactor using multiple lamps (2 or 4), which are located in an inner cylinder in the axis of the reactor [8]. In the hybrid, a pilot scale reactor of 11.4 m^3, the slurry is flowing through a multiple-lamp reactor and the catalyst is separated from the slurry using a membrane [9].

The author also concluded that a microreactor is a very promising photoreactor. A microreactor is a continuous tubular reactor with a volume of several microliters. The microreactor compared in the article had a volume of 1.49 µl. Although it was not fully optimized, the photo microreactor achieved the 4th highest PSTY. Table 1 shows that the lamp power was too high. If the power of the lamp was optimized, the PSTY would even be much higher than the PSTY of the pilot scale reactor. Another reason why this design is promising is the reaction rate. For the first time, reaction rate values on the order of magnitude 10 s^{-1} were reported when performing a first order reaction using a photo microreactor [6].

In industry, the throughput of a reactor is in order of $l.min^{-1}$. One single photo microreactor has a throughput in order of $ml.min^{-1}$. To increase the throughput with the intention to use photo microreactors in the industry, scaling-up is necessary. Numbering-up is in this case the most popular scale-up strategy. Using this strategy, a high amount of photo microreactors are distributed around the light source. Although the throughput is higher, the high reaction rates that were achieved will be lower due to the light that has to be distributed over the different reactors. Another possibility is to also number up the amount of light sources but this is often the most expensive component. Using photo microreactors, it is not possible to achieve a high throughput and a high reaction rate.

To solve this problem, a new method needs to be introduced to reach the industrial throughput and efficiently deliver enough light with the number of lamps as low as possible.

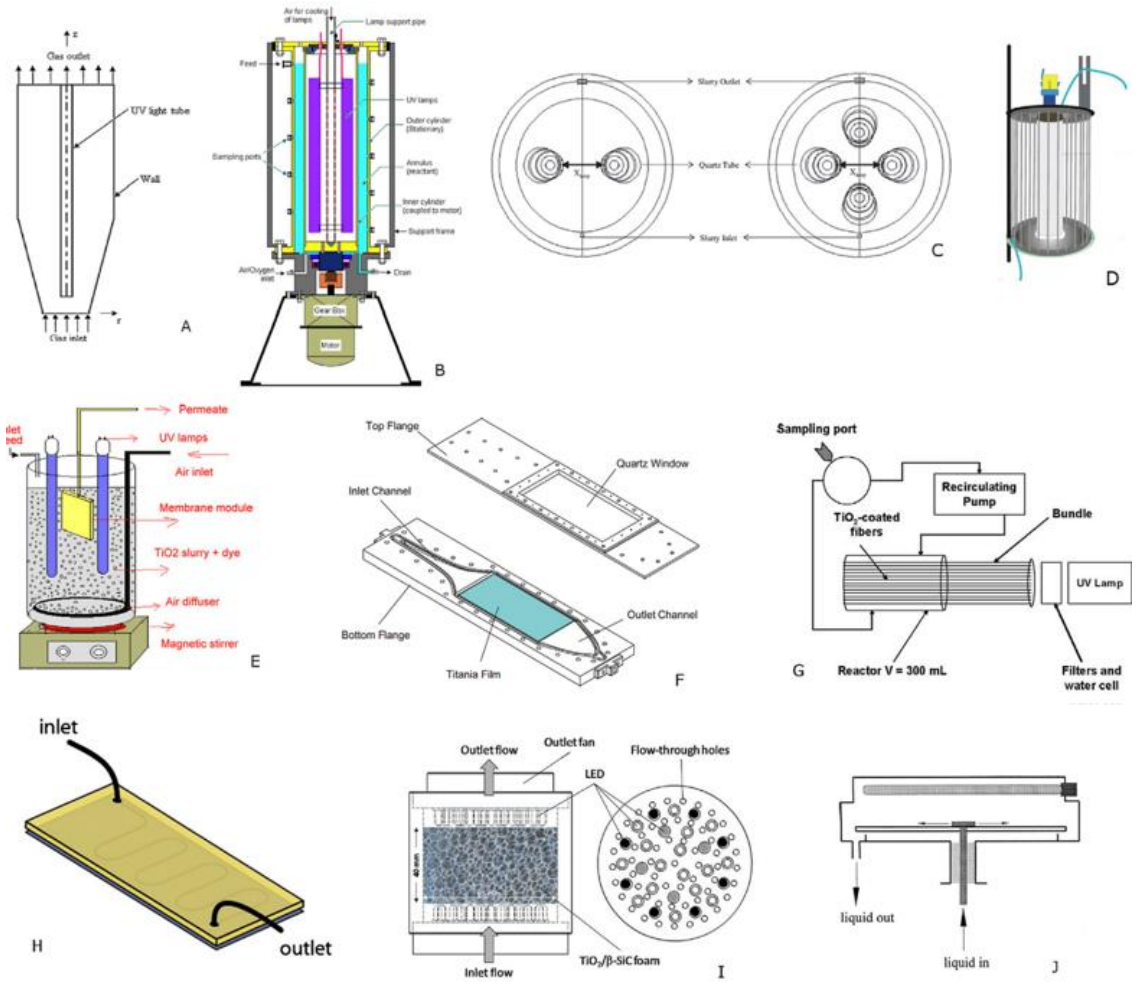

Fig. 3. (a) annular reactor(AR) [10], (b) rotating annular reactor(RAR) [11], (c) multi lamp reactor(MLR) [8], (d) capillary array reactor(CAP) [12], I photocatalytic membrane reactor(MEM) [7], (f) parallel plate reactor(PPL) [13], (g) optical fiber reactor(FIB) [14], (h) microreactor(MR) [6], (i) foam reactor(FR) [15], (j) spinning disk reactor(SDR) [16]

Table 1. PSTY data of the different photoreactor designs

	Reactor design	**V (m^3)**	**STY ($m^3\ m^{-3}$ reactor day^{-1})**	**LP (kW m^{-3} reactor)**	**PSTY ($m^3\ m^{-3}$ reactor $day^{-1}\ kW^{-1}$)**
Slurry	MEM/MLR	11.4	3.04	4.23	0.72
	MEM/MLR	0.135	1.44×10^{-2}	0.22	6.49×10^{-2}
	AR	8.0×10^{-4}	5.1×10^{-2}	500	1.0×10^{-4}
	RAR	7.6×10^{-3}	2.88×10^{-2}	15.8	1.83×10^{-3}
	MEM/AR	3.0×10^{-3}	0.1	155	6.52×10^{-4}
	CSTR	1.3×10^{-3}	0.123	1230	9.95×10^{-5}
	FR	1.0×10^{-3}	3.60×10^{-3}	32	1.13×10^{-4}
	SDR	1.0×10^{-2}	4.47×10^{-2}	3	1.49×10^{-2}
Immobilized catalyst	PPL	3.0×10^{-3}	3.60×10^{-2}	35	1.03×10^{-3}
	PPL	3.5×10^{-4}	3.03×10^{-2}	9.43	3.21×10^{-3}
	MR	1.5×10^{-9}	8.69×10^{5}	8.05×10^{7}	1.08×10^{-2}
	CAP	2.2×10^{-7}	5.85×10^{-3}	5.1×10^{4}	1.15×10^{-6}
	FIB	8.0×10^{-5}	4.80×10^{-4}	6.3×10^{3}	7.69×10^{-8}
	FR	5.0×10^{-5}	115	2.5 x 103	4.61×10^{-5}

2.3. Aerosol photoreactor

Among the photo microreactors, a novel micro structured reactor, aerosol photoreactor, is a quite promising candidate due to the possibility of this technology to boost the reaction rates and the throughput. Aerosol photoreactors use a nebulizer to nebulize the reaction medium with an inert or reacting gas as droplets of µm scale. Each droplet is working as a microreactor and will be irradiated by external light sources inside the reactor.

2.3.1. Aerosol

Aerosol is a suspension of solid or liquid particles in gas. Aerosols are usually stable for at least a few seconds and in some cases may last a year or more. Aerosol includes both the particle and the suspending gas. Spray aerosol is used in this thesis. Using this type, a droplet aerosol is formed by the mechanical breakup of a liquid. Particles are larger than a few micro meters [17].

There are two different ways to create a spray aerosol: a nebulizer and a nozzle, both shown in Fig. 4. When using a nozzle, an aerosol expands from a high-pressure reservoir through the nozzle into a low-pressure chamber. When using a nebulizer, compressed air is used to break up solutions into small aerosol droplets [18]. In this thesis, two types of nebulizers are used: a medical nebulizer and a continuous nebulizer. A medical nebulizer is connected to a compressor, which supplies air at a high velocity. The air is passed through a liquid solution to create an aerosol. A medical nebulizer creates a continuous flow of aerosol but needs to be refilled when empty. A continuous nebulizer, on the other hand, can create an aerosol continuously. The continuous nebulizer creates an aerosol using a parallel path method. Two different tubes are connected to the nebulizer, one with the liquid flow and one with the gas flow. This method enables the liquid to interact with the gas stream in the central portion of the gas stream. This causes the liquids to break up into smaller droplets in a continuous way.

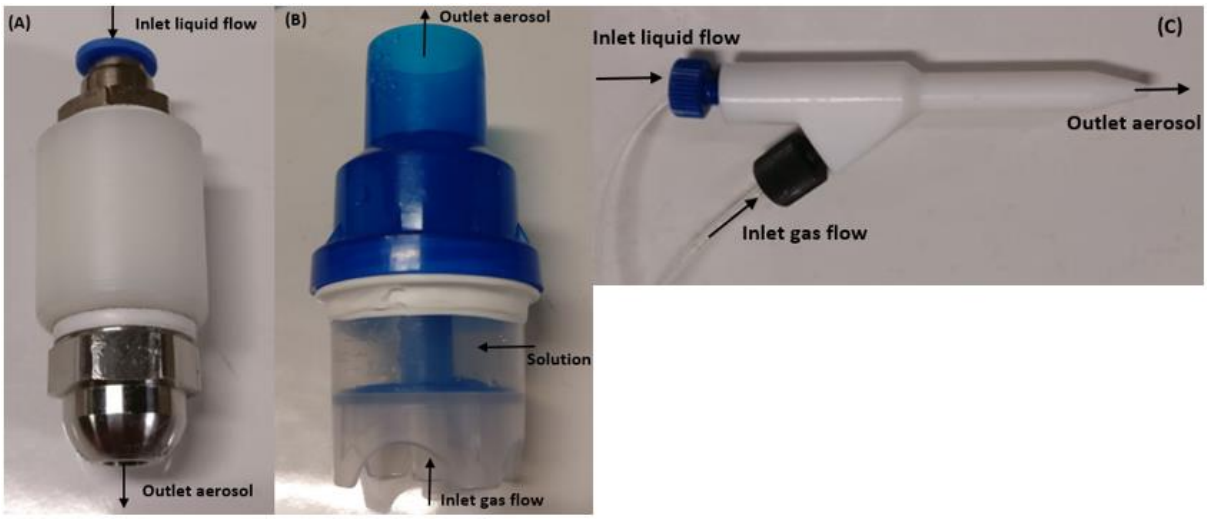

Fig. 4. (A) Nozzle, (B) Medical nebulizer, (C) Continuous nebulizer

An aerosol separation unit, to convert the aerosol back into liquid, has not been introduced yet. In this thesis, different separation units are tested.

2.3.2. Design and operation

To the best of my knowledge, an aerosol photoreactor has only been operated twice in literature. During one of the tests, the use of pneumatically generated aerosols concluded in a highly productive photooxidation. In the article a new kind of reactor design, an aerosol photoreactor, was introduced to solve the problems that occur when performing a photooxidation reaction in a standard continuous flow reactor: The poor oxygen solubility and the rapid attenuation of light when up-scaling the reactor [19].

The photooxidation reaction of β-citronellol was performed (Fig. 5), using the set-up that is shown in Fig. 6. The glass cylinder in the centre of the figure is the reactor where β-citronellol diluted with MeOH was sprayed into using a pneumatic nebulizer. Oxygen was used to create the aerosol. LED light tapes with a power of 10 $W.m^{-1}$ were mounted on the outside of the reactor to provide the light for the reaction. The end of the reactor was connected to two consecutive vessels placed in ice baths. On the second vessel, a water-cooled condenser was placed to prevent any product loss [19].

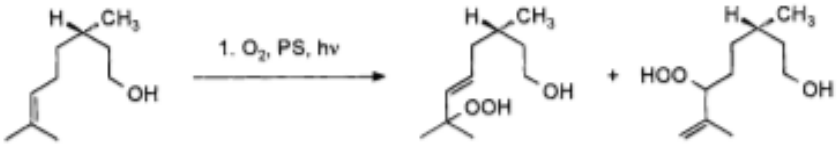

Fig. 5. Photooxidation reaction of beta-citronellol [20]

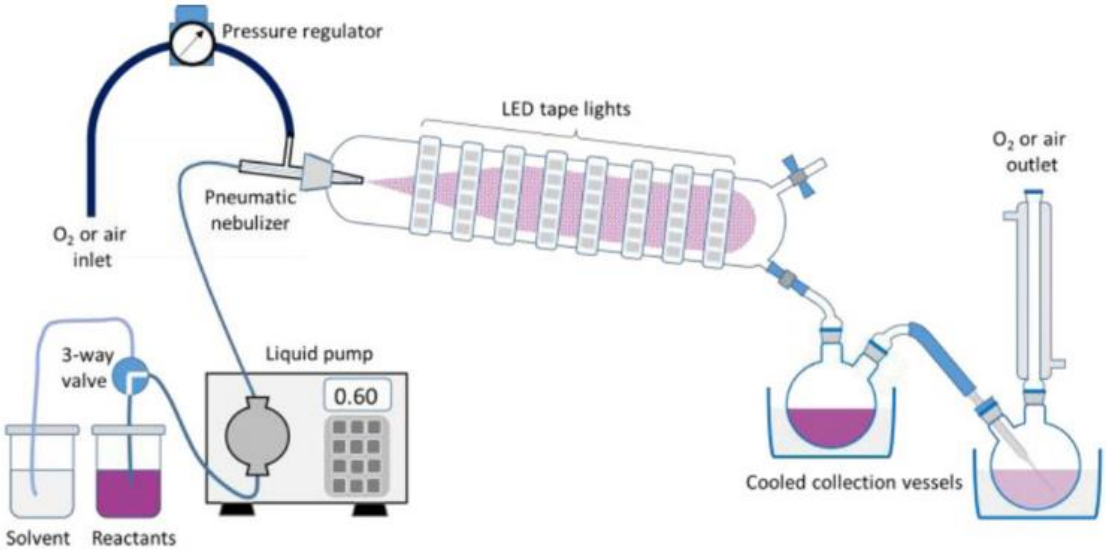

Fig. 6. Reactor design photooxidation reaction of beta-citronellol [19]

Different reagent concentrations and gas pressures were tested to see which combination(s) gave the best conversion and productivity. The productivity was calculated by the multiplication of the liquid flowrate, the concentration and the conversion. Table 2 gives an overview of the different combinations and the resulting conversions and productivities [19].

In general, high conversions were achieved with all the different combinations. When looking at the gas pressure for each concentration, it can be said that the higher the pressure, the higher the conversion was (except for 1.25 M). When looking at the solution concentration at a constant pressure, it can be said that the conversion was lower when the concentration was higher.

The productivity was high when comparing it with the liquid flowrate that was sprayed in the reactor (<1 ml/min). It didn't change that much when the gas pressure was changed at a constant concentration. The productivity was higher when the concentration of starting solution was higher at a constant pressure.

The results of this article displayed that an aerosol photoreactor is a very promising design however many things need to be done before it can be used in the industry. In the article, the authors were especially interested in the conversion of this reactor because it solved the problem of the low conversion in other types of reactors. Although the results were good, less information is given about the operation of the reactor. First of all, this reactor is a semi-continuous design, the reactor needs to be stopped to empty the collection vessels. To collect aerosol, the author uses collection vessels in ice baths. The efficiency of a collection vessel is the amount of liquid collected in the vessel compared to the amount of liquid in the reservoir at the start of the reactor. No info has been given about the efficiency of the collection vessels. The humidity inside the reactor can cause a decrease in efficiency of the collection vessels. Also no info has been given about the humidity. The residence time and the residence time distribution in the reactor is important when discussing a reaction but it is not mentioned in the article. Lastly, there is no info about the reliability of the LED strips that are mounted on the reactor and if they are used efficiently. In this thesis, a part of the improvement and characterization of those things is performed.

Table 2. Results photooxidation reaction of beta-citronellol

Concentration β-citronellol (M)	**Gas pressure (O_2) (psi)**	**Conversion (%)**	**Productivity (mmol.min^{-1})**
0.25	20	93	0.16
	30	91	0.19
	40	93	0.21
	50	95	0.20
	60	95	0.19
0.50	20	90	0.30
	30	87	0.36
	40	89	0.38
	50	93	0.40
	60	93	0.36
1.00	30	84	0.60
	40	89	0.71
	50	86	0.71
	60	92	0.69
1.25	40	82	0.70
	50	79	0.79

2.4. Residence time distribution

When modelling a reactor, the flow pattern is an important part. Different causes, for example channeling of fluid and the creation of stagnant regions in the vessel, will result in a deviation from the ideal flow pattern. There is a possibility to predict every deviation and so the behavior of a reactor but this prediction is impractical. In many cases, it is not necessary to know the precise behavior of the reactor. The residence time and the residence time distribution E (time^{-1}) help a lot [21]. The residence time is the time an individual molecule spends inside the system boundaries. The residence time distribution (RTD) is the distribution of residence times of the flowing fluids due to the different routes this fluid takes in the reactor [22]. Fig. 7 shows an example of an E-curve or RTD-curve. The RTD is presented in such a way that the area under the curve is equal to 1.

$$\int_0^\infty E\,dt = 1 \tag{6}$$

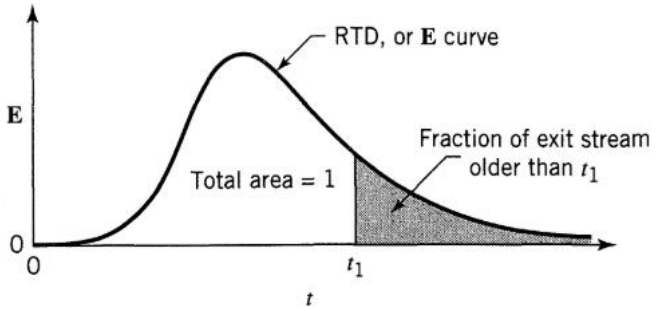

Fig. 7. RTD or E-curve [21]

Two experimental methods, using a non-reactive tracer, can be used to determine the RTD: a pulse experiment and a step experiment.

2.4.1. The pulse step experiment

When performing the pulse step experiment, M kg or mol of the non-reactive tracer is introduced in the reactor while it is running. At the end of the reactor, the concentration of tracer is measured in time. A C_{pulse}-curve is achieved as shown in Fig. 8a. Equation 7 and 8 respectively show the area under the C_{pulse}-curve (kg.s.m^{-3}) and the mean time that the tracer spends inside the reactor (s).

$$A = \int_0^\infty C\,dt \cong \sum_i C_i \Delta t_i = \frac{M}{v} \tag{7}$$

With *C* the concentration of tracer (mol.m^{-3} or kg.m^{-3}), *M* the amount of tracer introduced in the reactor (mol or kg) and *v* the flow rate inside the reactor (m³.s^{-1}).

$$\bar{t} = \frac{\int_0^\infty tC\,dt}{\int_0^\infty C\,dt} \cong \frac{\sum_i t_i C_i \Delta t_i}{\sum_i C_i \Delta t_i} = \frac{V}{v} \tag{8}$$

With *C* the concentration of tracer (mol.m^{-3} or kg.m^{-3}), *V* the volume of the reactor (m³) and *v* the flow rate inside the reactor (m³.s^{-1}).

To convert the C_{pulse}-curve into the E-curve or RTD-curve (Fig. 8b) divide the measured concentrations in time by M.v^{-1} as shown in equation 9.

$$E = \frac{C_{pulse}}{M/v} \tag{9}$$

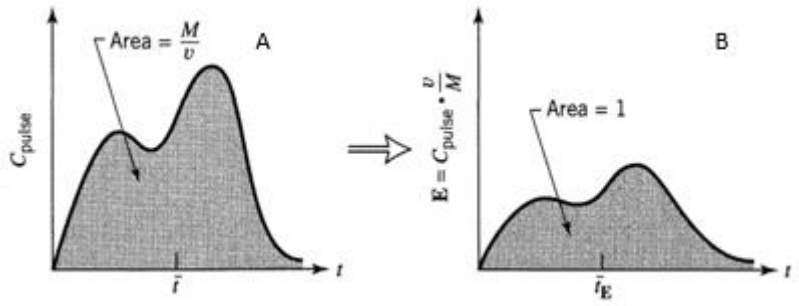

Fig. 8. Example of a C_{pulse}-curve (A) and an E-curve (B) [21]

2.4.2. The step experiment

A step experiment is almost comparable to a pulse step experiment. The only difference is the amount of tracer fluid that is introduced in the reactor. In a pulse step experiment, a known amount of tracer (M) is introduced in the reactor and measured at the outlet of the reactor. In a step experiment, at t=0, a switch is made from the continuously flow of ordinary fluid to a continuously flow of tracer fluid with a concentration of C_{max}. The concentration of tracer is measured at the outlet of the reactor in time and a C_{step}-curve is achieved as shown in Fig. 9a. Equation 10, 11 and 12 show respectively the calculation of maximum tracer concentration, The shaded area shown in Fig. 9a and the mean time the tracer fluid spends in the reactor.

$$C_{max} = \frac{\dot{m}}{v} \tag{10}$$

With C_{max} the maximum concentration of tracer in the outlet fluid ($kg.m^{-3}$), $\dot{m}$ the amount of tracer fluid entering the reactor ($kg.s^{-1}$) and v the flow rate of fluid inside the reactor (m^3/s).

$$A = C_{max}\bar{t} = \frac{\dot{m}V}{v^2} \tag{11}$$

With V the reactor volume (m^3)

$$\bar{t} = \frac{\int_0^{C_{max}} t\, dC_{step}}{\int_0^{C_{max}} dC_{step}} = \frac{1}{C_{max}} \int_0^{C_{max}} t\, dC_{step} \tag{12}$$

It is now possible to convert the C_{step}-curve into a dimensionless curve (Fig. 9b) by using equation 13. This curve is called a F-curve.

$$F = \frac{C_{pulse}}{\dot{m}/v} \tag{13}$$

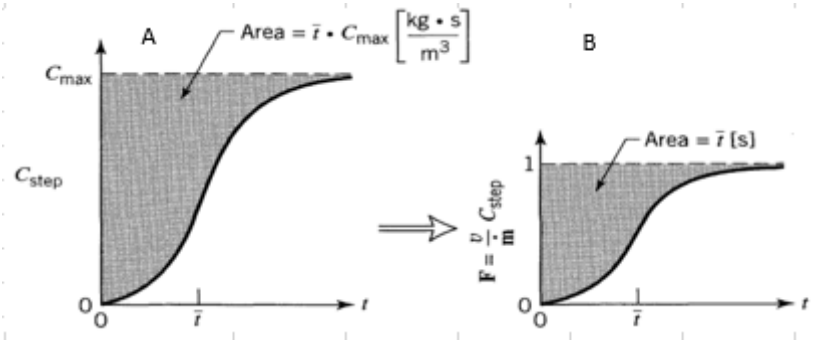

Fig. 9. Example of a C_{step}-curve (A) and a F-curve (B) [21]

The F-curve and the E-curve are related to each other by equation 14. The equation shows that at time t, the slope of the F-curve is equal to E. Using this equation, it is possible to create the E-curve as shown in Fig. 10.

$$\frac{dF}{dt} = E \tag{14}$$

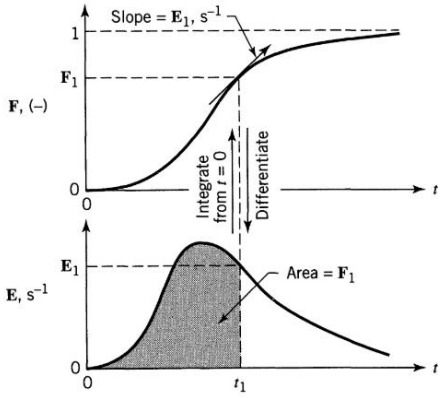

Fig. 10. Relation between E and F [21]

In this thesis, the RTD is determined for the continuous reactor using one of these methods.

3. Materials and methods

3.1. Batch to continuous set-up

During the experiments two reactors were used: a reactor using a medical nebulizer and a reactor using a continuous nebulizer i.e. Burgener Mira Mist nebulizer. A photo and process flow diagram of both reactors are shown in Fig. 11 and Fig. 12.

The reactor using a medical nebulizer was already installed at the start of the internship. The nebulizer had a reservoir of maximum 10 ml liquid. The reactor had a volume of 1860 ml. It used a Contimac CM 210/8/15 W BOXER compressor to supply the air for the aerosol formation. To regulate the air pressure of the compressor, a KelmK KFRS200-08-F-3 pressure regulator was used. The corresponding air flow rate was measured using a Kobold KDG-2242WV0000 rotameter.

During the internship, a TÜV SV 14 8-1 MS pressure safety valve was implemented in this set-up. It prevented a pressure build-up inside the reactor that could cause the reactor to fail. The gauge pressure was limited to 0.5 bar.

The reactor using a Burgener nebulizer was a new reactor that arrived during the internship. The Burgener nebulizer could create aerosol in specific ranges of gas and liquid flow rate. The range of the gas flow was 0.6-1.0 l/min, what corresponds to a pressure range of 2.41-3.10 bar for the compressor, and the range of the liquid flow was 0.2-2.5 ml/min. The reactor had a volume of 1910 ml. The set-up was assembled afresh after gathering the required components. It used the same compressor, pressure regulator and rotameter as the other reactor to supply the air for the aerosol formation. Unlike the other nebulizer, that had a reservoir of 10 ml, the Burgener nebulizer needed a continuous supply of liquid flow. A peristaltic pump, Watson Marlow 520S IP31, was added to the set-up to provide the liquid. To create a consistent flow without pulsations of the pump, a pulsation damper of 43.5 ml was connected after the pump. A Bronkhorst mini CORI-FLOW, which uses a PID, was implemented to regulate the flow of the peristaltic pump precisely. The pressure safety valve, also used in the other set-up, was added to complete the set-up.

After the set-up was completed, different gas and liquid flow rates were installed to check what happened inside the reactor. Gas flows of 2.50 bar and 3.00 bar were installed and liquid flow rates of 0.5 ml/min, 1 ml/min, 2 ml/min and 2.5 ml/min were installed.

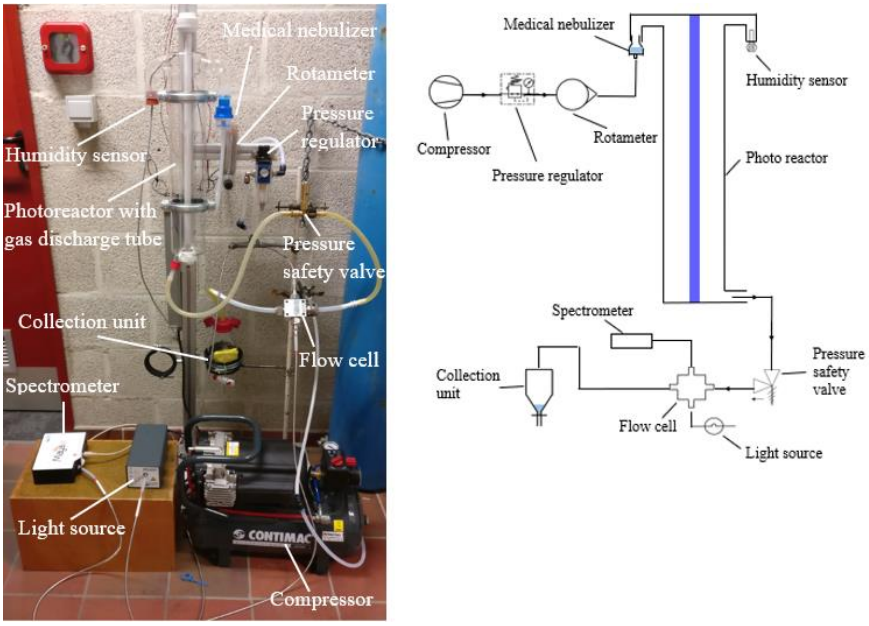

Fig. 11. Photo and process flow diagram of the reactor using a medical nebulizer

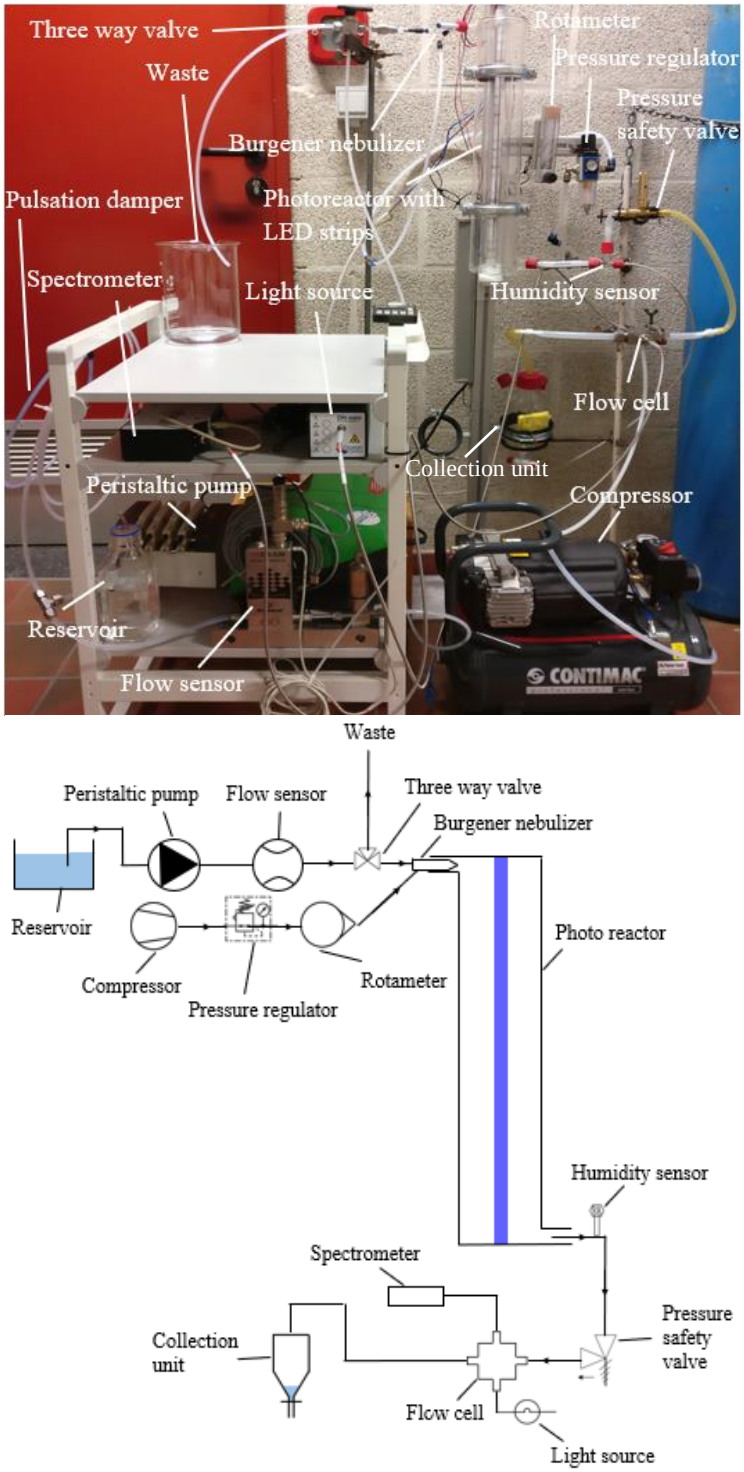

Fig. 12. Photo and process flow diagram of the reactor using a Burgener nebulizer

A humidity sensory, more specifically a Honeywell AIDC HIH-4000, was implemented at the end of the reactor using the continuous nebulizer to measure the humidity inside the reactor. The sensor was connected to an Arduino UNO and measured the relative humidity. The code used to measure the humidity can be found in the Appendix.

The humidity when only air is flowing in the reactor was measured first. When the humidity stayed constant, the aerosol flow with a gas pressure of 2.5 bar and a liquid flow of 2.5 ml/min was started. The humidity was then measured again and compared with the humidity when only air was flowing in the reactor.

3.2. Continuous phase separation operation

To separate the liquid from the aerosol flow at the outlet of the reactor, an appropriate filter was determined. Two types were tested: an hydrophilic glass frit and an hydrophobic polyethylene-filter. For both filter types, different pore sizes were tested. Table 3 gives an overview of the different filters and pore sizes and Fig. 13 gives an example of an hydrophilic frit and an hydrophobic PE-filter:

Table 3. Overview of the different filter types and pore sizes

Filter type	Designation	Filter size (µm)
Hydrophilic	P0	160-250
	P1	100-160
Hydrophobic	1	20-60
	2	40-100
	3	80-130

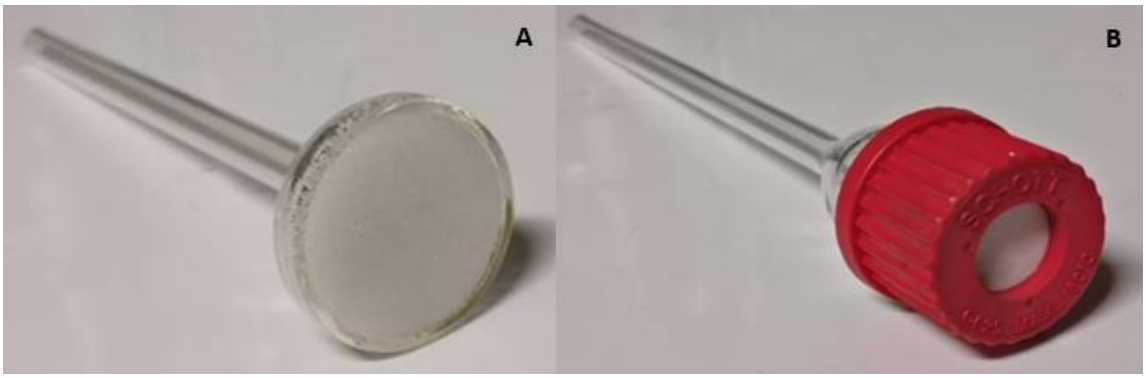

Fig. 13. A) Hydrophilic frit (100-160µm) B) Hydrophobic PE-filter (80-130µm)

The hydrophilic frits are designated according to the European standards. The hydrophobic filters are designated by self-chosen numbers.

To determine which filter gave the best results and is used to separate the aerosol flow in further experiments, the efficiency of each filter was calculated as shown in equation 15:

$$Efficiency = \frac{V_{collected}}{V_{start} - V_{end}} * 100 \quad (15)$$

With $V_{collected}$ the volume of water that was collected in the collection unit (ml), V_{end} the volume of water that was left in the reservoir of the nebulizer at the end of the run (ml) and V_{start} the volume of water in the reservoir at the start of each run.

The reactor using the medical nebulizer was used and V_{start} was equal to 7.5 ml. Each filter was tested at two different pressures, 1 bar and 2 bar. For each setting, a 20-minute run was performed three times. If the reservoir of the medical nebulizer was empty, the run was ended. At the end, an average of the three calculated efficiencies were taken. The filter with the best results for both pressures is used in further experiments.

3.3. Lamp reliability

To achieve a high PSTY, the optimization of the light source is important. Two light sources were tested: a Giesemann Super Actinic-T5-lamp, which is a gas-discharge tube, and Barthelme Y51515226 182003 LEDs. The fluctuations of these light sources in the length of the reactor and in time were determined. The absolute spectral irradiance of both sources, was measured using a Maya 2000pro spectrometer. The wavelength was varied between 200 nm and 1100 nm.

Table 4 and Fig. 14 give an overview of the measuring points spread over the length of the reactor starting from the top of the reactor. The absolute spectral irradiance of the six datapoints was measured three times on three different moments. For each dataset, an average was taken of the data in the range from 416.499 nm to 419.702 nm for the gas discharge tube and 540.376 nm to 560.590 nm for the LED strips. The maximum fluctuation of each dataset was calculated by subtracting the lowest irradiance value from the highest. When taking an average of the three obtained fluctuations, the fluctuation of the lamp in the length of the reactor was determined.

To determine the fluctuation in time, the spectral irradiance was measured every 5 minutes for 1 hour in point 4. This measurement was performed twice. For each dataset, an average was taken of the data in the range from 416.499 nm to 419.702 nm for the gas discharge tube and 540.376 nm to 560.590 nm for the LED strips. The fluctuation of each dataset was calculated by subtracting the lowest irradiance value from the highest. In the end, when for each lamp two fluctuations are calculated, an average of the two is taken and the fluctuation of the lamp in time was determined.

Table 4. Measuring points in the length of the lamp (starting from the top of the lamp)

Point on reactor	Length (cm)
1	4.5
2	11.0
3	18.0
4	25.0
5	33.0
6	41.0

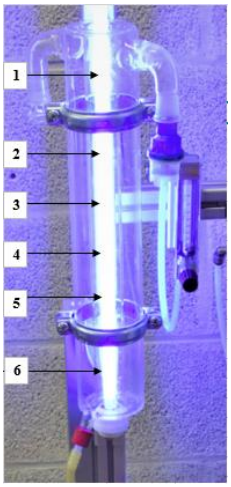

Fig. 14. Overview of the different measuring point

3.4. Residence time distribution

The residence time distribution was determined for the reactor using the continuous nebulizer by performing a step experiment. To perform the step experiment, a process Cross flow cell PRO-CFC-1-2 from Ocean Optics was implemented at the end of the reactor. A DH-mini light source and the Maya 2000pro spectrometer, measuring the transmission, were connected to the flow cell, perpendicular to the flow as shown in Fig. 15. The light path inside the flow cell was 5 mm. The integration time and the scans to average of the spectrometer were set to respectively 100 ms and 10. According to these settings, each second, one datapoint was taken.

At the start, only air was flowing through the reactor and flow cell. When the three-way valve was opened and water was provided to create aerosol, the measurement was started. The transmission decreased and when steady-state was achieved for at least 10 seconds, the measurement was stopped. As shown in Table 5, different gas pressures and liquid flow rates were tested. Each run was performed twice. An average was taken of the two calculated residence times.

The residence time distribution was calculated using the method that is mentioned earlier in the literature study. Because the transmission decreased during the experiments, the data was raised to the power of minus one to create the F-curve. Due to the large fluctuations in the data, the F-curve was smoothed by taking 10 averages. The slope was calculated in each point of the F-curve to achieve the E-curve and the residence time distribution. The peak in this curve indicates the average residence time.

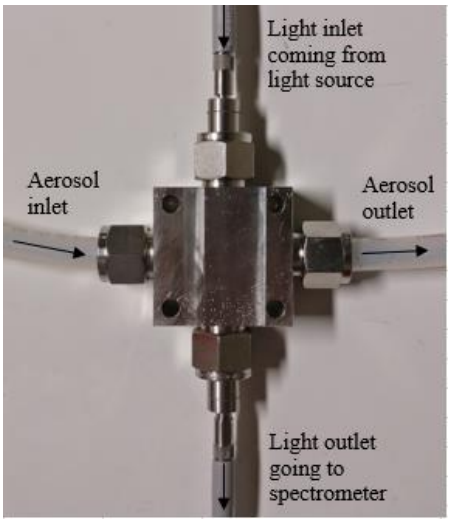

Fig. 15. Flow cell indicated with inlets and outlets of aerosol and light

Table 5. Parameter settings residence time distribution

Run	1	2	3	4	5
Air pressure (bar)	2.5	3.0	2.5	2.5	2.5
Air flow rate (ml/min)	600	1000	600	600	600
Liquid flow rate (ml/min)	2.5	2.5	2.0	1.5	1.0
Liquid/air ratio	0.0041	0.0025	0.0033	0.0025	0.0017

4. Results and discussion

4.1. Batch to continuous set-up

A continuous aerosol photoreactor has more benefits than a batch set-up. In a continuous reactor, it is possible to have a continuous production while in a batch set-up the reactor has to be shut down each time the reservoir is empty or the collection unit is full. When operating a reactor, it has to become steady-state and fully operative before a reaction can be performed. In a batch reactor, this process has to be repeated many times and is time consuming. In contrast to a batch reactor, a continuous reactor has to become steady state when it is operated for the first time and after maintenance.

To operate the continuous aerosol photoreactor smoothly, different components were gathered and implemented. The compressor, pressure regulator and rotameter, that were also used in the batch reactor, were implemented in this set-up to supply air continuously. A peristaltic pump, with a pulsation damper connected to it, was implemented to deliver a consistent liquid flow and a flow sensor with PID was implemented to regulate the liquid flow precisely. A pressure safety valve, humidity sensor and flow cell, used for the residence time distribution, were implemented without causing any problems.

Although the implemented components are working smoothly when operating the reactor, two problems occur. The first problem appears when spraying aerosol in the reactor. A part of the aerosol is sprayed directly into the wall of the reactor, is turned back into liquid and is captured at the bottom of the reactor. The remaining amount of aerosol is flowing down in a helix as expected. The helix will cause a higher residence time which results in a higher conversion. To solve the problem of the nebulizer spraying directly into the wall, different air pressures, liquid flow rates and nebulizer positions are tested but the same problem always occurs. A second problem is that no liquid is separated in the continuous separation unit. When operating the medical nebulizer with almost the same set-up, none of these problems occurs. These problems conclude that the Burgener Mira mist nebulizer is not suitable to produce aerosol in this set-up.

A new reactor concept that can be proposed using this nebulizer is a very small reactor. In an aerosol reactor, each droplet will operate as a microreactor. High reaction rates can be achieved with these kind of microreactors so less time is needed inside the reactor to achieve the same conversion as for example a slurry reactor. In a very small reactor, the Burgener nebulizer can create aerosol and spray it perpendicular against a wall. The aerosol passing can be illuminated with a light source. The time in the reactor will be very small but with the high reaction rates of the microreactors, the same conversion might be achieved. When spraying the Burgener nebulizer against the wall perpendicular from close distance, the liquid will be separated from the aerosol so a separation unit is not necessary, only a continuous collection unit.

Although this continuous nebulizer is not the right fit for this reactor, the method for the RTD-measurement is tried using this nebulizer because it can produce a continuous flow and the aerosol flow coming out of the reactor is enough to see a difference in transmission.

Inside the reactor, the evaporation of aerosol droplets is low. When only air was flowing in the reactor, the relative humidity was 21%. When introducing aerosol inside the reactor, the humidity immediately increased to 100%. This means the humidity inside the reactor is almost directly 100% and less evaporation of aerosol droplets will occur in the reactor.

4.2. Continuous phase separation operation

The results of the efficiency experiments of different filter types and sizes are shown in Table 6.

Table 6. Results efficiency experiments of different filter types and sizes

	Designation	Filter size (µm)	Pressure (bar)	Efficiency (%)
Hydrophilic	P0	160-250	1	20,0
			2	10,0
	P1	100-160	1	32,7
			2	43,3
Hydrophobic	1	20-60	1	Leakage due to backpressure
			2	
	2	40-100	1	
			2	
	3	80-130	1	44,0
			2	45,0

In general, all the filters have an efficiency lower than 50%. A first explanation for the low efficiency is the amount of water that is lost in the entrance of the reactor. The aerosol flow bounces against the glass wall and after some time, water droplets are formed. If the droplets are big enough, they will slide down the entrance wall back into the medical nebulizer and will be nebulized again. Although some of the liquid is flowing back into the medical nebulizer, some part of the liquid keeps sticking against the wall of the entrance what leads to losses in efficiency. Another explanation can be found in the medical nebulizer. It contains a bottom piece, which is the reservoir, and a top piece where the aerosol is expanded. After each experiment, the top piece contains water and it is not possible to measure this volume. The evaporation of aerosol droplets also leads to losses in efficiency. Due to the small droplet sizes of around 40µm, some of the aerosol is easily evaporated in the air. Although this is a reason for the lower efficiency, evaporation will influence the efficiency for a very small part. As discussed in the previous part, the humidity inside the reactor increases almost immediately to 100% if aerosol is introduced. If the humidity inside the reactor is 100%, the evaporation from aerosol droplets in the air is negligible.

The results show that hydrophilic frits designated with P0 have an efficiency of 20% and 10% for respectively 1 bar and 2 bar. The cause of these low values is the filter size. Due to the large glass particles, it is easier for the aerosol flow to pass through the frits. Also, the spaces in between the particle is bigger and because glass is a hydrophilic material, water is stored in the frits what leads to a loss in efficiency.

The hydrophobic filters designated with 1 and 2 have no results. Due to the small particle size of the filter, the backpressure is too high what creates leakages in the medical nebulizer.

The hydrophilic frit designated with P1 and the hydrophobic filter designated with 3 have similar results. The lower efficiency of the hydrophilic frit at 1 bar can be explained by the frit that was not fully saturated yet. Although both filters have advantages and disadvantages, the hydrophilic frit will be used in the collection unit from now on due to their chemical inertness. They are also cheaper and easier to buy. To saturate the frit with water, two options are possible. If the hydrophilic frit is not implemented in the set-up before the experiments, it is possible to submerge it in water and saturate it. If the frit is already implemented, it takes 30 minutes to saturate it using aerosol.

4.3. Light reliability

Fig. 16 and Table 7 give an overview of the different measuring points and the corresponding length starting from the top of the reactor. Fig. 17 shows an example of a spectrum of the gas discharge tube (A) and the LED strips (B). Both spectra are taken in point four. Fig. 17 (C) and (D) give a representation of the spectra taken in the length of the reactor, zoomed in on the range in where the average is taken to calculate the total fluctuation of the lamp in the length. The X-axis represents the wavelength (nm) and the Y-axis the absolute spectral irradiance (µW/cm².nm).

Table 7. Measuring points in the length of the lamp (starting from the top of the lamp)

Point on reactor	Length (cm)
1	4.5
2	11.0
3	18.0
4	25.0
5	33.0
6	41.0

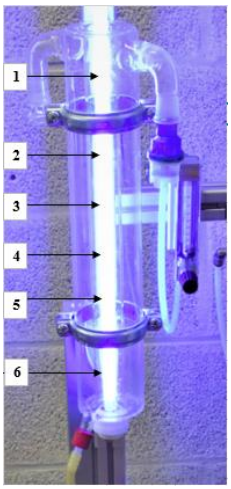

Fig. 16. Overview of the different measuring point

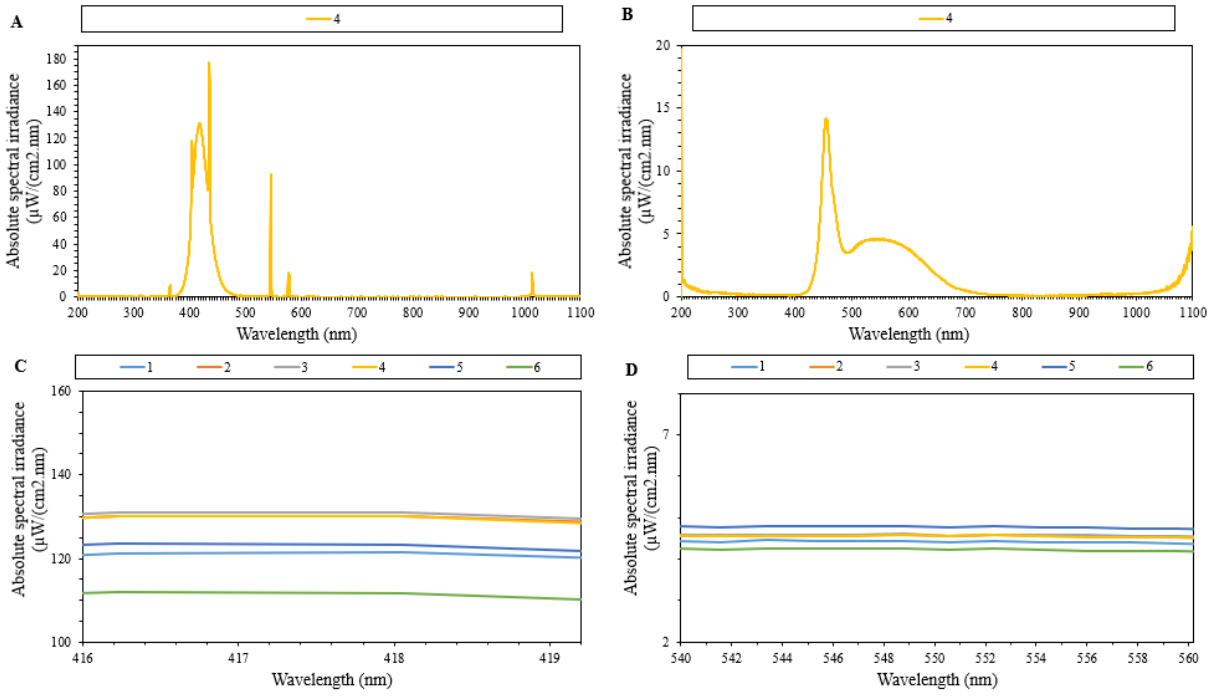

Fig. 17. A) Spectrum gas discharge tube B) Spectrum LED strips C) Spectrum 6 points in the length of the gas discharge lamp D) Spectrum 6 points in the length of the LED strips

As shown in Fig. 17, the absolute spectral irradiance of the gas discharge tube is much higher than the irradiance of the LED strips. This can be explained by looking at the power of both lamps. the gas discharge tube has a power of 80 W while each LED has a power of 0.24 W and all the LEDs used in the reactor have a total of 6 W. Fig. 18 shows the average irradiance in each measuring point for both lamps, Fig. 19 shows an average of the maximum fluctuation in the length for both lamps.

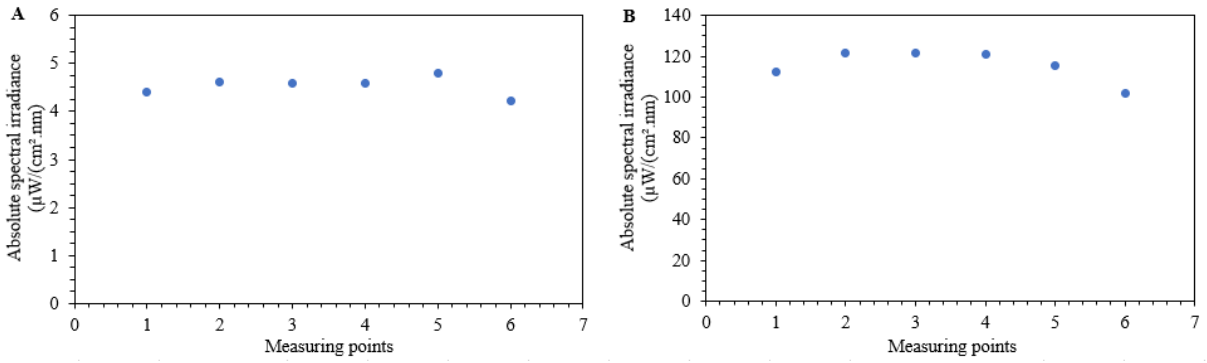

Fig. 18. The average irradiance in each measuring point for A) LED strips B) gas-discharge tube

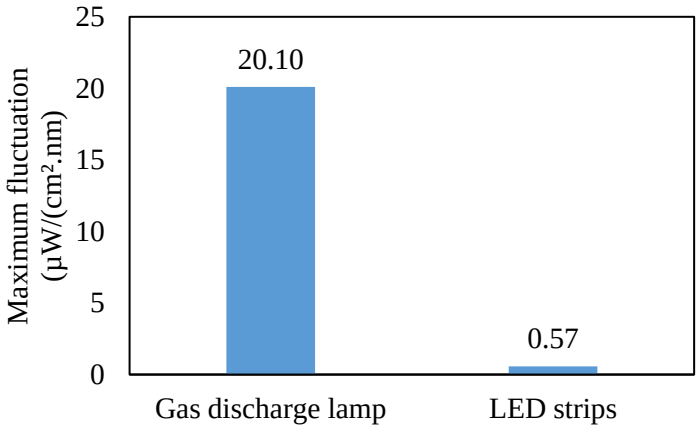

Fig. 19. Maximum fluctuation in length

For all the runs, studying the gas discharge tube, the maximum irradiance difference was measured between point three (18 cm) and six (41 cm). For the LED strips, the maximum irradiance difference was measured between point five (33 cm) and six (41 cm). As shown in Fig. 19, the maximum irradiance difference is 20.10 µW/(cm².nm) with a standard deviation of 0.82 for the gas discharge lamp and 0.57 µW/(cm².nm) with a standard deviation of 0.03 for the LED strips. Fig. 20 shows the average fluctuation of the irradiance in time for 1 hour in point four for both lamps.

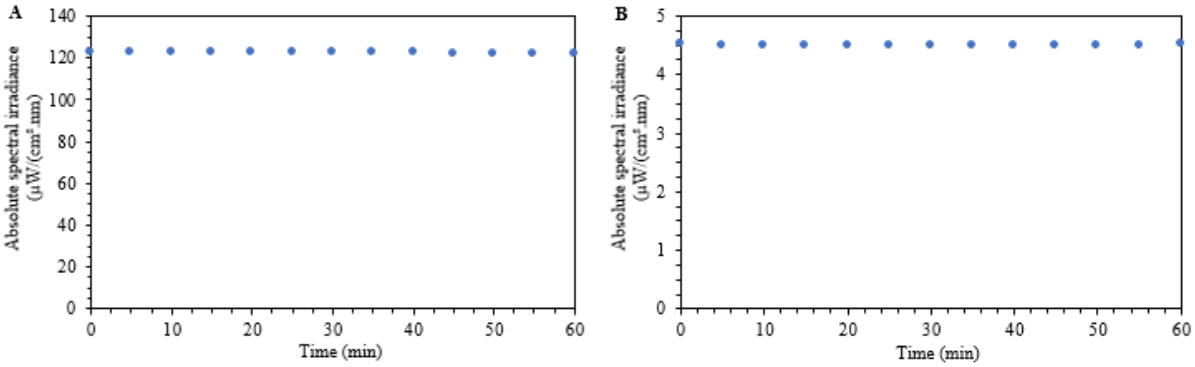

Fig. 20. Average irradiance in function of the time A) gas discharge tube B) LED strips

When analyzing Fig. 20, The absolute spectral irradiance is almost constant in time. The maximum irradiance difference in time is 0.78 µW/(cm².nm) for the gas discharge tube and 0.0092 µW/(cm².nm) for the LED strips. Those changes in irradiance are negligible when comparing them with the differences in the length of the reactor.

When dimming the light to achieve a higher efficiency, this irradiance difference has to be taking into account so the absolute spectral irradiance is not zero at some points in the reactor. Because point six always has the lowest absolute spectral irradiance, the light can be dimmed according to this point. The irradiance in the other measuring points will be higher and the highest spectral irradiance will be measured in point five for the gas discharge tube and point three for the LED strips.

4.4. Residence time distribution

The F-curve, represented in Fig. 21, shows that the measurement of the transmission is a good method to measure the RTD. In an ideal plug flow reactor (PFR), the step in the F-curve will appear immediately. Although all engineers aim to create an ideal plug flow reactor, it is impossible. The higher the slope of the step-curve, the more the reactor can be shown as a PFR. When the slope is less, the reactor is more a continuous stirred tank reactor (CSTR).

Fig. 21 shows the comparison of the F-curves when changing the gas pressure from 3.0 bar to 2.5 bar.

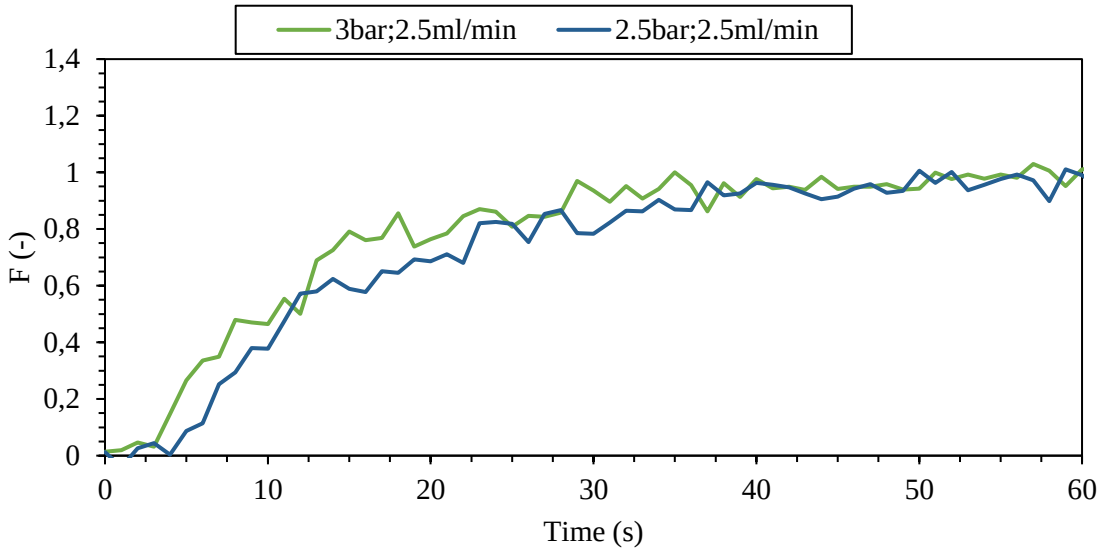

Fig. 21. Comparison of the F-curves when changing the gas pressure

When decreasing the gas pressure, the gas flow rate is decreased and the step-curve is not as steep. The gas flow rate is almost 1 l/min at 3 bar and almost 0.6 l/min at 2.5 bar. The difference in gas flow rate is not that high, that is why the difference in the slope is also not that high. The decrease in slope concludes that when the gas pressure is decreased, the reactor is more a CSTR. A decrease in the slope of the step-curve can be explained by the shear forces inside the reactor. At the reactor wall, the velocity of aerosol is zero. The velocity will increase while moving to the middle of the two walls of the reactor. Because the velocity in the middle is higher than on the wall, the aerosol droplets in the middle will leave the reactor earlier than the droplets closer to the wall. This will cause the step-curve to be less steep. The lower the gas flow rate, the lower the velocity inside the reactor and the higher the difference between the velocity in the middle and the velocity closer to the wall. Due to the higher difference in velocity, it takes longer for the aerosol droplets closer to the wall to leave the reactor and it takes longer to come to steady state what results in a step-curve that is less steep. When looking at the F-curves, it can be predicted that the average residence time ,when the air pressure is higher, will be lower.

When comparing different liquid flow rates, as shown in Fig. 22, The difference in the slope of the four curves is small. This means the slope is only affected by the gas flow rate and not by the liquid flow rate. The liquid flow rate will affect the droplet size. When looking at the F-curves, similar results are achieved. According to this data, it can be said that the average residence time will not change much when changing the liquid flow rate.

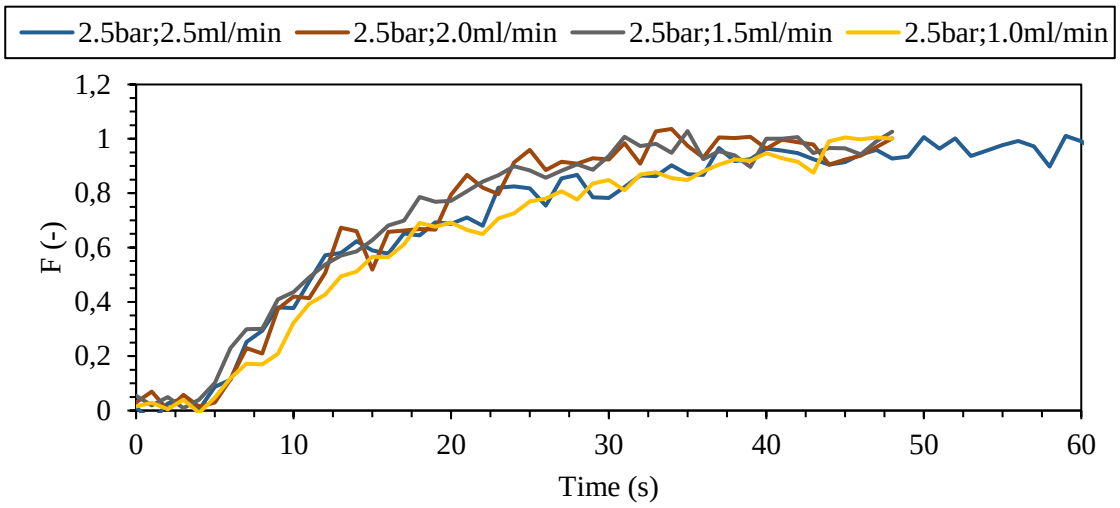

Fig. 22. Comparison of the F-curves when changing the liquid flow rate

After measuring the residence time distribution (RTD) for the different parameters mentioned in the methods and materials, one problem occurred during the calculation: the fluctuations of the spectrometer are high. Due to the high fluctuations, it is not possible to calculate the E-curve starting from the F-curve. Fig. 23 shows an example of a F-curve and E-curve a gas pressure of 3 bar and 2.5 ml/min liquid flow rate.

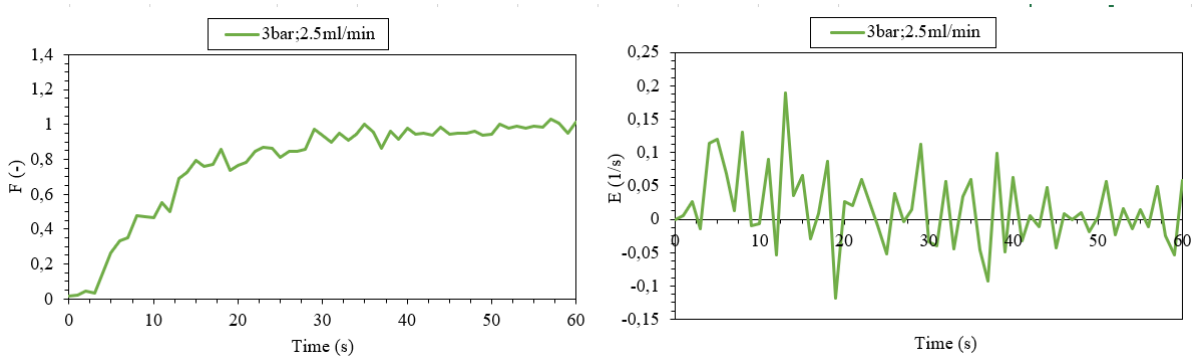

Fig. 23. F-curve and E-curve RTD-measurement

Due to the fluctuations in the F-curve, it is not possible to take the derivative in each point of the graph. When looking at the E-curve, many peaks appear and even negative E-values are calculated. Even after smoothing the F-curve, it is not possible to determine the average residence time. To solve this problem, it is possible to take more datapoints with the spectrometer. During the experiment, an average of 10 data points was taken by the program which concludes in 1 datapoint each second. By lowering the amount of data points that are averaged by the program, more datapoints can be achieved. Lowering the averaging of datapoints will not decrease the fluctuations in the transmission.

The fluctuations in transmission can be caused by different things. In the flow cell, glass plates are mounted on the parts where the light source and spectrometer are connected. Aerosol droplets can cause condensation on the glass plates what can cause fluctuations in the transmission. An hydrophobic coating can be applied on the glass surface so no droplets can stick on the surface. Droplets not following the helix flow can be another reason of the fluctuations. Some droplets can immediately flow to the outlet of the reactor. This problem can be solved by implementing a baffle inside the reactor so the aerosol droplets are required to follow the helix flow. The continuous nebulizer that is unsuitable for the set-up can be a last cause of the fluctuations. The liquid sliding down the wall and the liquid collected in the bottom of the reactor can manipulate the aerosol flow and cause the fluctuations. To solve this problem, another type continuous nebulizer has to be implemented in the set-up.

5. Conclusion

This thesis shows that a transformation from batch to a continuous aerosol photoreactor is possible when using another type of continuous nebulizer.

The humidity inside the continuous reactor increases immediately to 100 % when providing aerosol in the reactor. Once the humidity is 100 %, the loss of aerosol droplets to evaporation is very small.

Hydrophilic filters with a particle size of 100-160 µm and hydrophobic filters with a particle size of 80-130 µm have the same efficiency results. Due to the chemical inertness and lower cost, hydrophilic filters are the most suitable to use in the continuous phase separation operation. Although in the continuous reactor no liquid could be collected, an efficiency of 43.3 % is achieved when using the medical nebulizer set-up.

An absolute spectral irradiance difference of maximum 20.10 µW/(cm².nm) is measured between point three (18 cm) and point six (41 cm) for the gas-discharge tube. An absolute spectral irradiance difference of maximum 0.57 µW/(cm².nm) is measured between point five (33 cm) and point six (41 cm). The irradiance difference in time is for both light sources negligible. The lamp can be dimmed efficiently according to point six since the lowest irradiance values are measured here.

Lastly, it was not possible to calculate the precise average residence time in the continuous reactor due to data fluctuation. When looking at the F-curves, the average residence time is lower when the gas pressure is 3 bar. When the gas pressure is 3 bar, the step-experiment is closer to a plug flow reactor then at 2 bar. The liquid flow rate does not affect the residence time distribution. More datapoints can solve the problem to calculate the average residence time although smoothing of the data is necessary. To create less fluctuations in data, coating the glass plates of the flow cell with an hydrophobic material can be a solution.

References

[1] M. E. Leblebici, B. Van den Bogaert, G. D. Stefanidis, and T. Van Gerven, “Efficiency vs. productivity in photoreactors, a case study on photochemical separation of Eu,” *Chem. Eng. J.*, vol. 310, pp. 240–248, 2017.

[2] R. W. Ditchburn, *Light*, Third. Academic press, 1976.

[3] A. Smale, “Electromagnetic Spectrum - Introduction,” 2013. [Online]. Available: https://imagine.gsfc.nasa.gov/science/toolbox/emspectrum1.html. [Accessed: 12-Apr-2019].

[4] D. F. Swinehart, “The Beer-Lambert Law,” *J. Chem. Educ.*, vol. 39, no. 7, pp. 333–335, 2009.

[5] M. E. Leblebici, G. D. Stefanidis, and T. Van Gerven, “Comparison of photocatalytic space-time yields of 12 reactor designs for wastewater treatment,” *Chem. Eng. Process. Process Intensif.*, vol. 97, pp. 106–111, 2015.

[6] A. Visan, D. Rafieian, W. Ogieglo, and R. G. H. Lammertink, “Modeling intrinsic kinetics in immobilized photocatalytic microreactors,” *"Applied Catal. B, Environ.*, vol. 150–151, pp. 93–100, 2014.

[7] R. A. Damodar and S. You, “Performance of an integrated membrane photocatalytic reactor for the removal of Reactive Black 5,” *Sep. Purif. Technol.*, vol. 71, pp. 44–49, 2010.

[8] Y. Boyjoo, M. Ang, and V. Pareek, “CFD simulation of a pilot scale slurry photocatalytic reactor and design of multiple-lamp reactors,” *Chem. Eng. Sci.*, vol. 111, pp. 266–277, 2014.

[9] M. J. Benotti, B. D. Stanford, E. C. Wert, and S. A. Snyder, “Evaluation of a photocatalytic reactor membrane pilot system for the removal of pharmaceuticals and endocrine disrupting compounds from water,” *Water Res.*, vol. 43, no. 6, pp. 1513–1522, 2009.

[10] N. Qi, H. Zhang, B. Jin, and K. Zhang, “CFD modelling of hydrodynamics and degradation kinetics in an annular slurry photocatalytic reactor for wastewater treatment,” *Chem. Eng. J.*, vol. 172, no. 1, pp. 84–95, 2011.

[11] M. Subramanian and A. Kannan, “Photocatalytic degradation of phenol in a rotating annular reactor,” *Chem. Eng. Sci.*, vol. 65, no. 9, pp. 2727–2740, 2010.

[12] Z. Zhang, H. Wu, Y. Yuan, Y. Fang, and L. Jin, “Development of a novel capillary array photocatalytic reactor and application for degradation of azo dye,” *Chem. Eng. J.*, vol. 184, pp. 9–15, 2012.

[13] M. Vezzoli, W. N. Martens, and J. M. Bell, “General Investigation of phenol degradation: True reaction kinetics on fixed film titanium dioxide photocatalyst,” *"Applied Catal. A, Gen.*, vol. 404, no. 1–2, pp. 155–163, 2011.

[14] A. Danion, J. Disdier, C. Guillard, F. Abdelmalek, and N. Jaffrezic-renault, “Characterization and study of a single-TiO2-coated optical fiber reactor,” *Appl. Catal. B*, vol. 52, pp. 213–223, 2004.

[15] N. Doss, P. Bernhardt, T. Romero, R. Masson, V. Keller, and N. Keller, “Photocatalytic degradation of butanone (methylethylketone) in a small-size TiO2/B-SiC alveolar foam LED reactor,” *"Applied Catal. B, Environ.*, vol. 154–155, pp. 301–308, 2014.

[16] H. C. Yatmaz, C. Wallis, and C. R. Howarth, “The spinning disc reactor - studies on a novel TiO2 photocatalytic reactor,” *Chemosphere*, vol. 42, pp. 397–403, 2001.

[17] W. Hinds, “Aerosol Technology,” *Mater. Res. Bull.*, vol. 31, no. 3, pp. 342–343, 2002.

[18] S. K. Friedlander, Smoke, Dust, and Haze, *Fundamentals of Aerosol Dynamics*, vol. 2. 2000.

[19] S. A. Pergantis, T. Montagnon, G. Vassilikogiannakis, D. Kalaitzakis, and G. I. Ioannou, "A Novel Nebulizer-Based Continuous Flow Reactor: Introducing the Use of Pneumatically Generated Aerosols for Highly Productive Photooxidations," *ChemPhotoChem*, vol. 1, no. 5, pp. 173–177, 2017.

[20] R. Gerdes, O. Bartels, G. Schneider, D. Wöhrle, and G. Schulz-Ekloff, "Photooxidations of Phenol, cyclopentadiene and citronellol with photosensitizers ionically bound at a polymeric ion exchanger," *Polym. Adv. Technol.*, vol. 12, no. 3–4, pp. 152–160, 2001.

[21] O. Levenspiel, *Chemical Reaction Engineering*, Third. John Wiley & Sons, 1999.

[22] E. B. Nauman, "Residence time theory," *Ind. Eng. Chem. Res.*, vol. 47, no. 10, pp. 3752–3766, 2008.

Appendix

```
int analogPin = A0; //connect brown wire to A0 // connect orange wire to ground and connect the green wire with 5V
float humidity = 0;

void setup(){
Serial.begin(9600);

void loop(){
float humidity = ((analogRead(A0) * (5.0 / 1023.0))-0.826)/0.0315;
Serial.println(humidity);
delay(1000);
}
```

Fig. 24. Arduino code to measure humidity in the reactor